General theory of nonlinear flow-distributed oscillations

Patrick N. McGraw and Michael Menzinger
Department of Chemistry, University of Toronto, Toronto, Ontario, Canada M5S 3H6
(Received 24 February 2003; revised manuscript received 26 August 2003; published 30 December 2003)

We outline a general theory for the analysis of flow-distributed standing and traveling wave patterns in one-dimensional, open flows of oscillatory chemical media, emphasizing features that are generic to a variety of kinetic models. We draw particular attention to the cases far from a Hopf bifurcation and far from the so-called kinematic or zero-diffusion limit. We introduce a nonlinear formalism for both traveling and stationary waves and show that the wave forms and their amplitudes depend on a single reduced transport parameter that quantifies the departure from the kinematic limit. The nonlinear formalism can be applied to systems with more complex types of bifurcations (canards, period doublings, etc.).

DOI: 10.1103/PhysRevE.68.066122 PACS number(s): 82.40.Ck, 47.70.Fw, 05.45.−a

I. INTRODUCTION

The flow-distributed oscillation (FDO) [1–16] mechanism of spatial pattern formation was predicted in one-dimensional chemical flows [1,2] and subsequently experimentally verified in the Beluosov-Zhabotinsky (BZ) reaction [3–5]. FDO differs from the Turing [17] and related mechanisms [18] and from the differential flow instability [19,20] in that it does not require any differential transport of the reacting species. This mechanism operates in open flow systems when the chemical kinetics is intrinsically oscillatory and the inflow boundary condition plays an essential role. Its possible relevance to biological pattern formation (e.g., somitogenesis and axial segmentation) has been suggested, since an open flow system is related by a coordinate transformation to an axially growing medium such as a plant stem or animal embryo [11–14]. Key features shared with other open flow systems in fluid mechanics and plasma physics [21–25] are convective instability, broken reflection symmetry, and the important role of boundary conditions in pattern selection. Chemical FDO was originally analyzed using a linear stability analysis of an unstable fixed point of the chemical dynamics [1,2]. As pointed out in Ref. [9], the linearized analysis is most useful when the kinetic system is not far from a supercritical Hopf bifurcation. Likewise, the frequently studied complex Ginzburg-Landau equation [21–23] describes the amplitude dynamics of weakly nonlinear waves. Chemical oscillators, however, have interesting dynamical regimes far from a Hopf bifurcation, showing strongly nonlinear oscillations. In such cases, the fixed point enclosed by the limit cycle may be an unstable node rather than a focus, in which case a linearized analysis does not reveal the intrinsic oscillatory behavior at all. A helpful intuitive view of the nonlinear FDO is provided by considering the kinematic or zero-diffusion limit [7] in which the FDO represents a straightforward mapping of the chemical temporal dynamics onto the flow axis. The kinematic picture, however, misses some essential features, including the extinction of the waves under sufficiently strong diffusion.

The goal of this paper is to outline a general framework for for understanding both stationary and traveling FDO waves, especially in cases where neither the linear analysis nor the kinematic picture gives an adequate description of the fully developed waves. Unlike some of the fluid dynamics or plasma physics examples of convective instabilities, the medium considered here is intrinsically oscillatory even in the absence of a flow and there is no differential transport. We are primarily interested in the conditions under which steady waves propagate and in the wave forms of those waves. We consider sinusoidal boundary conditions which select a particular wave frequency, rather than noise-sustained structures in which the boundary condition is noisy and the pattern is selected by the response of the medium itself [28,23]. Our attention is devoted more to steady patterns than to the moving fronts that invade the unstable medium. A general discussion of such fronts is given in [22] and some discussion of those fronts in the case of FDO is given in [10].

In Sec. II we introduce the governing equations of FDO and discuss the kinematic limit, which provides an intuitively simple starting point for describing strongly nonlinear FDO waves, although we shall be interested particularly in deviations from the kinematic limit. In Sec. III we discuss the linear stability analysis of a fixed point with emphasis on generic features of the two types of fixed points, unstable foci and unstable nodes. Analyzing the response to time-dependent perturbations imposed at the inflow, we show that a band of frequencies is spatially amplified and that this band becomes narrower and sharper with increasing diffusion. We derive general expressions for the thresholds separating absolute from convective instability as well as the threshold for extinction of stationary waves and show that the latter threshold disappears in the case of an unstable node (a typical case far from a Hopf bifurcation). In the latter case we also show that, in contrast to previous examples, sustained stationary waves can arise through an absolute instability from a transient perturbation rather than from a steady boundary perturbation. In Sec. IV we use a traveling wave ansatz to introduce a reduced one-dimensional ordinary differential equation (ODE) that describes the fully nonlinear stationary and traveling waves. Numerical solutions of this equation are easier to obtain than those of the partial differential equation and they allow us to obtain the *dispersion relation* for the fully developed, large amplitude waves. A key result is that the amplitude and shape of the wave depend only on the reduced transport parameter $\Gamma \equiv D/(v-c)^2$,

where c is the phase velocity of the wave. It is Γ that governs the strength of deviations from the kinematic limit. We show that in the case of relaxation or strongly nonlinear oscillations these deviations are qualitatively different from those in the quasisinusoidal case, and we provide a physical interpretation of the dependence on Γ. We illustrate the application of our techniques with some numerical results. Finally, in Sec. V we summarize our conclusions and describe the prospects for applying our techniques to more complex types of bifurcations (canards, period doublings, etc.) in open flow systems.

Throughout the paper we use as an illustrative model the van der Pol or FitzHugh-Nagumo (FN) oscillator [18,26,27]

$$\frac{dX}{dt} = e(X - X^3 - Y),$$

$$\frac{dY}{dt} = -Y + 10X, \tag{1}$$

which is described in more detail in Appendix A. The FN model exhibits the generic features we are interested in: it provides examples of quasisinusoidal oscillations changing to relaxation oscillations and an unstable focus changing to an unstable node as e is increased. Appendix B describes the numerical approaches used and the challenges encountered in solving the one-dimensional ODE described in Sec. IV.

II. THE KINEMATIC LIMIT

The governing equations of the one-dimensional open reactive flow studied are the reaction-diffusion-advection (RDA) equation

$$\frac{\partial \mathbf{U}}{\partial t} = \mathbf{f}(\mathbf{U};C) - v\frac{\partial \mathbf{U}}{\partial x} + D\frac{\partial^2 \mathbf{U}}{\partial x^2} \tag{2}$$

together with the boundary condition $\mathbf{U}(0,t)$ at the inflow. Here $\mathbf{U}(x,t)$ is an N-dimensional vector of dynamical variables (concentrations of species), $\mathbf{f}(\mathbf{U};C)$ is the vector-valued rate function which depends on one or more control parameters C, $v>0$ is the flow velocity, and D is the diffusion coefficient. In general D and v can be matrices, allowing for differential transport, but here we focus on the case without differential transport, so that v and D are real scalars. We take the length of the reactor to be L and impose no-flux boundary conditions at the outflow: $\partial U/\partial x|_{x=L}=0$. We are interested in the case where $\mathbf{f}(\mathbf{U};C)$ has a stable limit cycle and at least one unstable fixed point.

In the diffusionless or *kinematic* limit [7] Eq. (2) can be written as

$$\frac{d\mathbf{U}}{dt} = \mathbf{f}(\mathbf{U};C), \tag{3}$$

where we have introduced the advective derivative $d/dt \equiv \partial/\partial t + v\,\partial/\partial x$. In this limit each fluid element is an independent oscillator, and the inflow boundary condition serves to establish the phase of these oscillators [3]. If the boundary condition is constant, for example, then all of the oscillators enter the reactor with the same initial phase and stationary waves result from the recurrence of the same phase at equally spaced downstream positions. On the other hand, an oscillating boundary condition leads to upstream or downstream traveling waves, which have also been verified experimentally [11–16]. The wavelengths and phase velocities of waves generated by forcing the boundary at a given frequency can be derived simply by requiring that the phase of of each advected fluid element increase by 2π during each time interval of $T_0 = 2\pi/\omega_0$, where ω_0 is the natural frequency of the chemical oscillator. The dispersion relation is $\omega = \omega_0 + vk$ and the phase velocity c as a function of frequency is given by

$$c = v\left(\frac{\omega_0}{\omega_0 - \omega} + 1\right). \tag{4}$$

Two features of these relations are physically instructive. First, as $\omega \to \omega_0$ the wavelength and phase velocity become infinite. This wave corresponds to a synchronous oscillation of the entire medium. Second, as $\omega \to \pm\infty$, the wavelength becomes small and the phase velocity approaches the flow velocity, corresponding to an imposed spatial pattern passively transported with the flow. The kinematic limit is helpful for understanding the essential physics, but diffusion introduces mixing between adjacent fluid elements which may be oscillating out of phase and alters the wavelengths [6] as well as the amplitudes and shapes of flow-distributed waves [4]. Sufficiently strong diffusion may extinguish the waves. The strength of diffusion effects depends on the magnitude of the spatial gradients. The kinematic viewpoint leads one to expect diffusion to play a stronger role as the flow velocity decreases, or as the driving frequency becomes large, since both tend to lead to shorter wavelengths. We will show in Sec. IV that this is correct and that the strength of deviations from the kinematic limit can be quantified by a single reduced flow parameter.

III. GENERIC LINEARIZED ANALYSIS NEAR A FIXED POINT

In the linearized approximation, a small perturbation $\mathbf{U}(x,t) = \mathbf{U}_0 + \mathbf{u}(x,t)$ of the unstable fixed point $\mathbf{U}_0$ obeys

$$\frac{\partial \mathbf{u}}{\partial t} = \mathbb{J}(\mathbf{U}_0)\mathbf{u} - v\frac{\partial \mathbf{u}}{\partial x} + D\frac{\partial^2 \mathbf{u}}{\partial x^2}, \tag{5}$$

where $\mathbb{J}$ is the Jacobian matrix $\partial \mathbf{f}(\mathbf{U})/\partial \mathbf{U}$. Denoting the eigenvectors and eigenvalues of the Jacobian by ξ_j and $\lambda_j = \alpha_j + i\beta_j$, respectively ($j \in \{1,\ldots,N\}$) and expanding

$$\mathbf{u}(x,t) = \sum_{j=1}^{N} u_j(x,t)\,\xi_j \tag{6}$$

gives a separate equation for each component:

$$\frac{\partial u_j}{\partial t} = (\alpha_j + i\beta_j)u_j - v\frac{\partial u_j}{\partial x} + D\frac{\partial^2 u_j}{\partial x^2}. \tag{7}$$

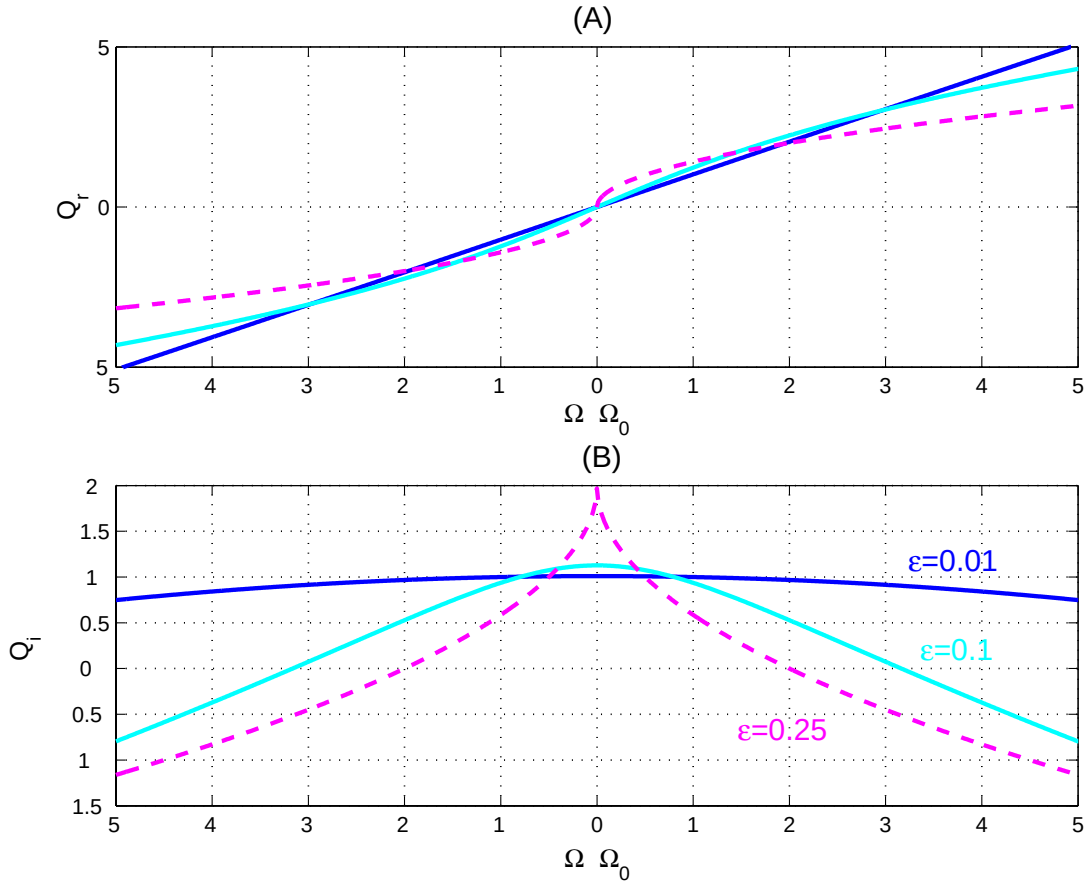

FIG. 1. (Color online) General solutions to the dispersion relation near an unstable fixed point. (a) Real part of the wave number; (b) imaginary part. The band of spatially growing modes ($Q_i>0$) becomes sharper with increasing ε.

We are interested in unstable eigenvectors for which $\alpha>0$. (In the following we suppress the subscript j.) Without loss of generality we assume $\beta\geqslant 0$. In the case where $\mathbf{U}_0$ is an unstable node, which frequently occurs far from a Hopf bifurcation, we have $\beta=0$. Substitution of a complex exponential $u(x,t)=A\exp(i\omega t-ikx)$ into Eq. (7) gives the dispersion relation

$$i\omega=\alpha+i\beta+iUk-Dk^2. \tag{8}$$

To analyze the dispersion relation generically, it is convenient to use the dimensionless quantities $\Omega\equiv\omega/\alpha$, $Q=Q_r+iQ_i\equiv Uk/\alpha$, $\varepsilon\equiv D\alpha/U^2$, and $\Omega_0\equiv\beta/\alpha$. We now restrict our attention to purely real frequencies, an appropriate restriction when the boundary is forced sinusoidally with a steady amplitude. In dimensionless variables, the real and imaginary components of the dispersion relation (8) read

$$Q_i+\varepsilon(Q_r^2-Q_i^2)=1, \tag{9}$$

$$Q_r-2\varepsilon Q_rQ_i=\Omega-\Omega_0. \tag{10}$$

In general these equations possess two solutions. As discussed in [23], in the presence of quite general downstream boundary conditions it is the solution with the *less positive* (i.e., more slowly growing) value of Q_i that dominates in the bulk. Numerical solutions for Q_r and Q_i as functions of $\Omega-\Omega_0$ for the relevant branch are plotted in Fig. 1 for several values of ε. It is easy to show that $Q_i>0$ (i.e., perturbations grow with downstream distance) when

$$-\frac{1}{\varepsilon}<\Omega-\Omega_0<\frac{1}{\varepsilon}, \tag{11}$$

and the maximum growth rate always occurs at $\Omega=\Omega_0$. The onset of absolute instability occurs when $\varepsilon=1/4$ and is marked by the appearance of a cusp in Q_i and a vertical jump in Q_r at $\Omega=\Omega_0$. The absolute instability threshold can also be derived by considering the group velocity $d\omega/dk$ of propagating disturbances [2,8,29,30]. Absolute instability occurs when a disturbance propagates upstream and grows with time; thus the threshold of this instability occurs when the mode with zero group velocity has precisely zero growth rate ($\omega_i=0$). The first mode to cross the absolute instability threshold is always the Hopf mode $\Omega=\Omega_0$.

An important special case, most commonly probed in experiments and previous simulations, is that of a fixed boundary condition which results in stationary waves ($\Omega=0$). From Eq. (11) we see that stationary waves grow if $\Omega_0<1/\varepsilon$ and are evanescent otherwise. This result together with the threshold $\varepsilon=1/4$ for absolute instability allow one easily

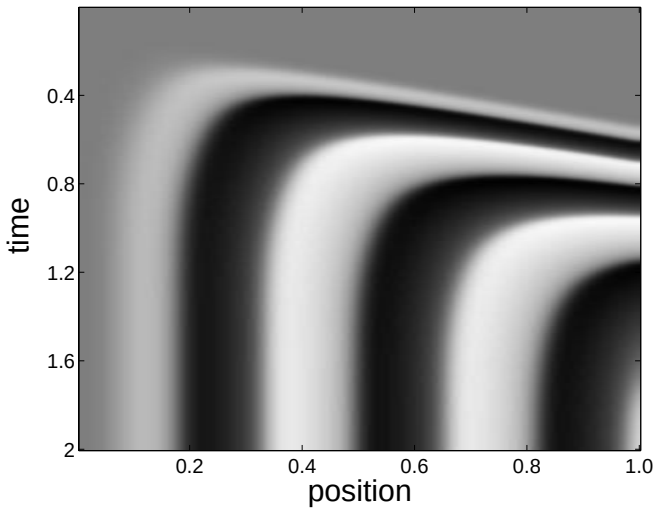

FIG. 2. Onset of absolute instability in the FN system. The gray levels are proportional to $X(x,t)$. The inflow boundary conditions are $X(0,t)=-0.001$, $0<t<0.1$, $X(0,t)=0$ otherwise. The unstable fixed point (0,0) is a node under the conditions $e=50$, $v=1$, $D=0.01$.

to plot curves for these thresholds as functions of flow and kinetic parameters for an arbitrary system, generalizing the results of [2] and [8].

The above results remain valid if the unstable fixed point is a node rather than a focus, i.e., $\Omega_0=0$, as frequently occurs in chemically inspired models which are far from a Hopf bifurcation, although the waves described are qualitatively somewhat different. In this case, the fastest growth is along the most unstable eigendirection. A stationary wave mode is always the most unstable mode, and the first mode to cross the absolute instability threshold. This mode initially grows as a pure spatial exponential with a purely imaginary wave number, but when the amplitude grows large enough for nonlinear terms to be significant a finite-wavelength oscillation takes over. There are no evanescent stationary waves. (The disappearance of the evanescent wave region was observed in Refs. [2,8,9] but not extensively remarked upon.) Figure 2 shows an example of a numerical simulation[1] in which a stationary wave pattern arises via an absolute instability rather than through a steady boundary perturbation, in sharp contrast to previous examples [8,9].

IV. NONLINEAR, LARGE AMPLITUDE WAVES

In this section we derive a reduced ordinary differential equation that describes both stationary and traveling wave solutions of the RDA equation (2) and applies to situations where neither the linear stability analysis nor the kinematic limit give an adequate description. We show that the amplitude and wave form depend on a single reduced transport parameter which characterizes the degree of departure from the kinematic limit. The application of our formalism is then illustrated by some numerical examples. As in the linearized analysis, we find that the two cases near and far from a Hopf bifurcation give qualitatively different wave behavior. The latter case departs significantly from what the linear stability analysis would lead one to expect.

We make the ansatz $\mathbf{U}(x,t)=\mathbf{U}_c(x-ct)$, which is analogous to the D'Alembert solution of the wave equation. It represents a generic wave (not necessarily periodic) traveling downstream with velocity c and depending only on the combination $\zeta\equiv x-ct$. A growing or decaying traveling wave is not strictly described by this ansatz unless $c=0$ (since a spatially changing amplitude implies a dependence on x and not purely on ζ), but we expect that it describes the asymptotic behavior of such a wave when the amplitude saturates. Substituting this into the reaction-diffusion-advection equation (2) gives a one-dimensional ODE:

$$0=\mathbf{f}(\mathbf{U})-(v-c)\frac{\partial\mathbf{U}}{\partial\zeta}+D\frac{\partial^2\mathbf{U}}{\partial\zeta^2}. \tag{12}$$

With a change of variable $\zeta'\equiv\zeta/(v-c)$ we obtain

$$0=\mathbf{f}(\mathbf{U})-\frac{d\mathbf{U}}{d\zeta'}+\Gamma\frac{d^2\mathbf{U}}{d\zeta'^2}, \tag{13}$$

where

$$\Gamma\equiv\frac{D}{(v-c)^2}. \tag{14}$$

Γ represents the effective strength of the diffusion term for a given wave. If Eq. (13) has a periodic solution $\mathbf{U}(\zeta')=\mathbf{U}(\zeta'+\Lambda)$, then the period Λ in terms of ζ' is related to the frequency and wave number of the corresponding traveling wave by

$$\omega=ck=\frac{c}{(c-v)}\frac{2\pi}{\Lambda(\Gamma)}, \tag{15}$$

where we have made explicit the dependence of Λ on Γ.

For a physical interpretation of the particular combination of parameters Γ, it is helpful to consider again the intuition developed in Sec. II based on the kinematic limit. First, note that $\Gamma\to 0$ as $|v-c|\to\infty$. The limits $c\to\pm\infty$ (infinite phase speed) both correspond to synchronous oscillations in which there are no spatial gradients. Diffusion has no effect in this limit and the system behaves like a well-mixed one. Alternatively, as $v\to\infty$ the wavelengths in the kinematic picture become large, the spatial gradients are small, and little diffusive mixing occurs between adjacent crests and troughs. On the other hand, as c approaches v from either direction Γ diverges, as decreasing $|v-c|$ tends to compress the waves.

If the underlying chemical dynamics is not far from a supercritical Hopf bifurcation, then $\mathbf{f}(\mathbf{U})=\mathbf{f}(\mathbf{U}_0+\mathbf{u})$ can be

[1]Numerical solutions of the RDA equation were obtained using a simple first-order discretization. The time and space grids were adjusted according to the characteristic time and space scales of the system being studied. For a sufficiently fine grid, the results were verified to be insensitive to the grid size.

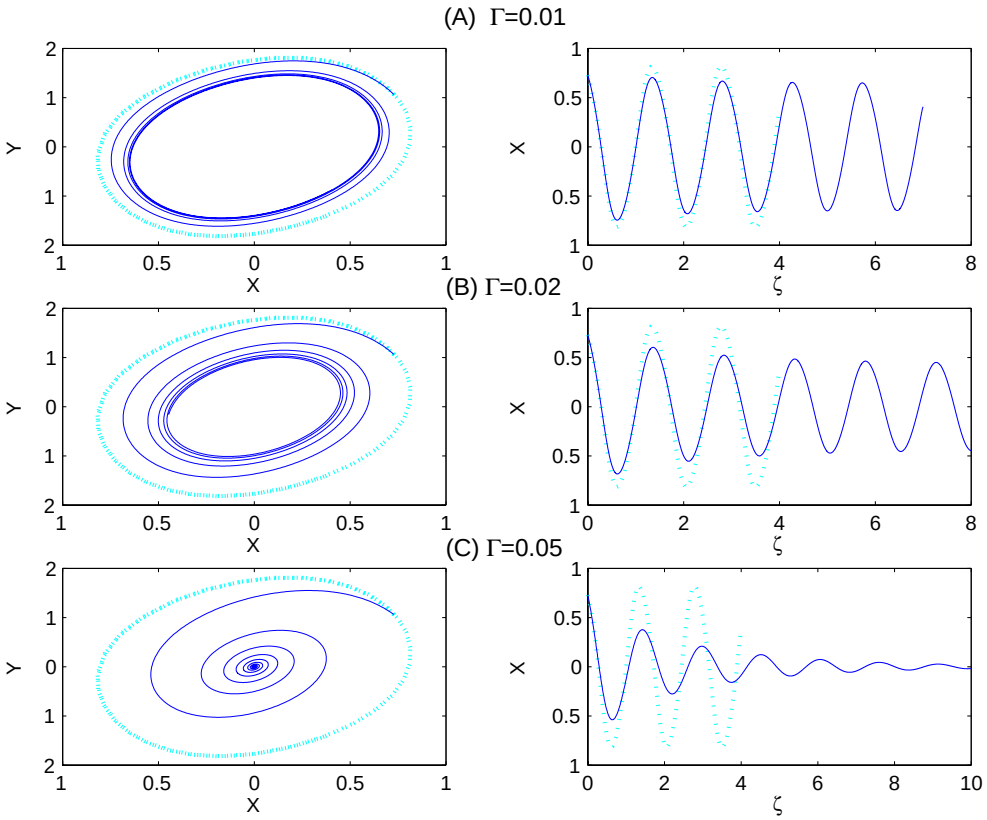

FIG. 3. (Color online) Numerical solutions of Eq. (13) for the FN system with $e=2$. The left column shows $Y(\zeta)$ vs $X(\zeta)$, the right shows $X(\zeta)$ vs ζ. The dotted and lighter-colored curves show solutions in the kinematic limit (or $\Gamma=0$). The boundary conditions are fixed at a point on the local limit cycle at one end, free at the other end. In this weakly nonlinear regime Γ functions like a Hopf bifurcation parameter: for $\Gamma<0.28$ [(a) and (b)] there is a periodic quasisinusoidal wave form, but for $\Gamma>0.28$ (c) the solution spirals into the origin. The period changes little as Γ increases.

approximated by a cubic function and it can then be shown that periodic solutions with finite amplitude exist only if

$$\Gamma=\frac{D}{(v-c)^2}<\frac{\alpha}{\beta^2}. \tag{16}$$

Γ thus functions as a bifurcation parameter for a Hopf-like bifurcation of a particular wave mode.

As a special case, when $c=0$ we recover the previous result for the threshold for the extinction of stationary waves. In the weakly nonlinear case when $\beta>0$, Eq. (16) predicts that traveling waves with phase speeds close to the flow velocity do not propagate. Waves with sufficiently small amplitude are well described by the linearized dispersion relation of Sec. III. The cutoff frequency predicted by Eq. (11) is precisely the frequency at which the resulting traveling waves reach the threshold phase velocity set by Eq. (16). For the case of an unstable node or $\beta=0$, on the other hand, the threshold (16) diverges and so it appears that there is no excluded band of phase velocities, and waves may propagate arbitrarily close to the flow velocity. The case of strongly nonlinear waves in a case far from a Hopf bifurcation is considered below.

A. Numerical solutions and qualitative features of nonlinear wave forms

Equation (13) is useful for several reasons. First, it shows that the essential features of traveling and stationary waves (the amplitude and the wave form) depend on a single combination of transport parameters, Γ, and therefore a family of different waves are described by a single universal function. Second, as a general rule, ODE's can be solved with less computational effort than partial differential equations (PDE's), and Eq. (13) allows one to derive wave solutions without solving the full PDE (2). Solution methods are described in Appendix B.

Some examples of numerical solutions for the FN system are shown in Figs. 3 and 4. As expected, increasing Γ has the general effect of increasing the deviations from the kinematic limit. However, the behavior differs qualitatively between the quasisinusoidal and the relaxation oscillation cases. In the former case, the phase space orbit remains approximately elliptical. Its period remains approximately constant while its amplitude shrinks uniformly until, at the critical threshold $\Gamma=\alpha/\beta^2$, it vanishes into the fixed point. In the relaxation oscillation case, on the other hand, the limit cycle does not shrink to a point. Instead, as Γ increases, the period Λ increases apparently without bound, and the limit cycle re-

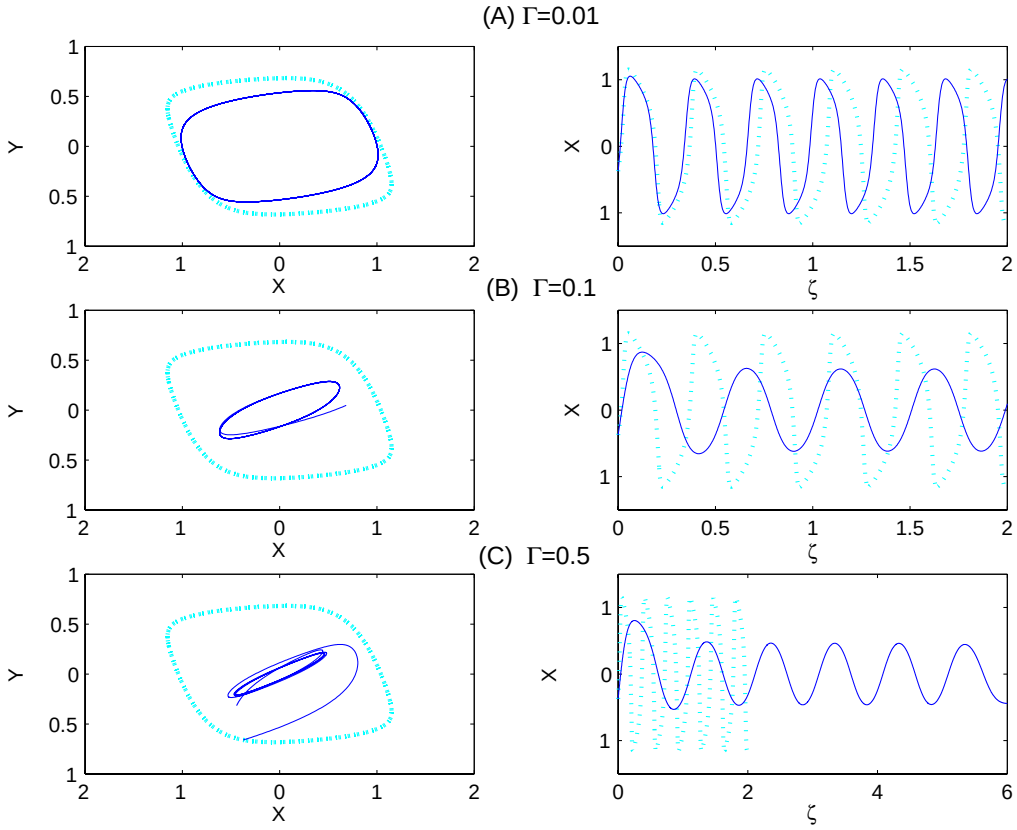

FIG. 4. (Color online) Solutions of Eq. (13) as in Fig. 3 but for $e=50$. As Γ increases, the period lengthens compared to the kinematic limit, and the wave forms trace narrower loops in phase space, but they do not spiral into the origin at any finite Γ.

mains elongated in the more unstable eigendirection while narrowing in the transverse direction.

B. Dispersion relation for nonlinear waves

By finding $\Lambda(\Gamma)$ numerically for a range of values of values of Γ and then using the relation (15) together with the definition $\Gamma=D/(v-c)^2$, one can find the *nonlinear dispersion relation* between the frequency ω (which can be set by the forcing frequency of a perturbation at the inflow) and the phase velocity c of large amplitude traveling waves at given values of the transport parameters D, v. We have done this for the FN model at two values of e and plotted the results in Fig. 6 below. In the quasisinusoidal dynamical regime near the Hopf bifurcation, Λ is nearly constant and approximately equal to the small amplitude oscillation period $2\pi/\beta$. The ω-c relation is then approximately the same as that predicted in the kinematic limit, except that it is truncated at the cutoff frequencies $\beta\pm\sqrt{\alpha v^2/D}$ [see Fig. 6(b)]. Outside this interval of frequencies there are only evanescent waves.

In the strongly nonlinear regime, on the other hand, Λ varies quite strongly with Γ. In fact, numerical results suggest that for asymptotically large Γ it increases approximately linearly (see Fig. 5). This means that the frequency does not become infinite as $c\to v$ but instead reaches a maximum. Such a maximum is seen in Fig. 6(a), which shows frequency versus phase speed for the case $e=50$, $D=0.003$, $v=1$, based on the numerical data for $\Lambda(\Gamma)$. This relation is radically different from the one for small amplitude, linearized waves. The maximum frequency appears to be lower than the cutoff frequency obtained from the linear stability analysis. There is thus a range of frequencies for which the linear theory predicts a growing mode, yet there are no large amplitude solutions described by Eq. (13) cor-

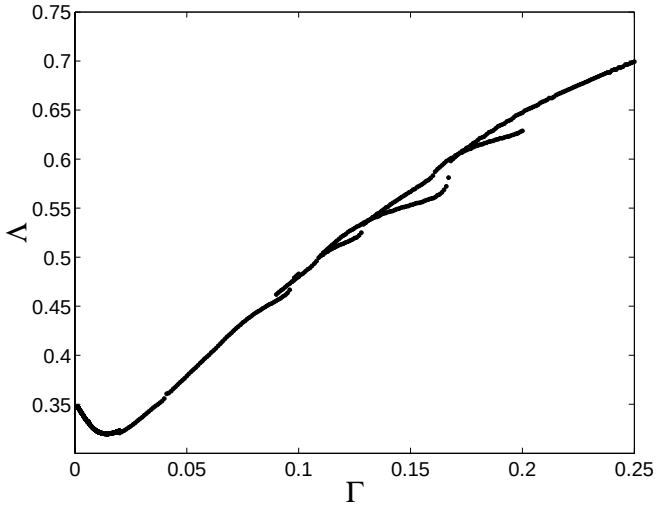

FIG. 5. Scaled wavelength Λ as a function of Γ obtained from numerical solutions of the one-dimensional equation. Λ appears to increase approximately linearly for large Γ. The numerical results become more uncertain at longer wavelengths due to the finite interval of the solution (see Appendix B).

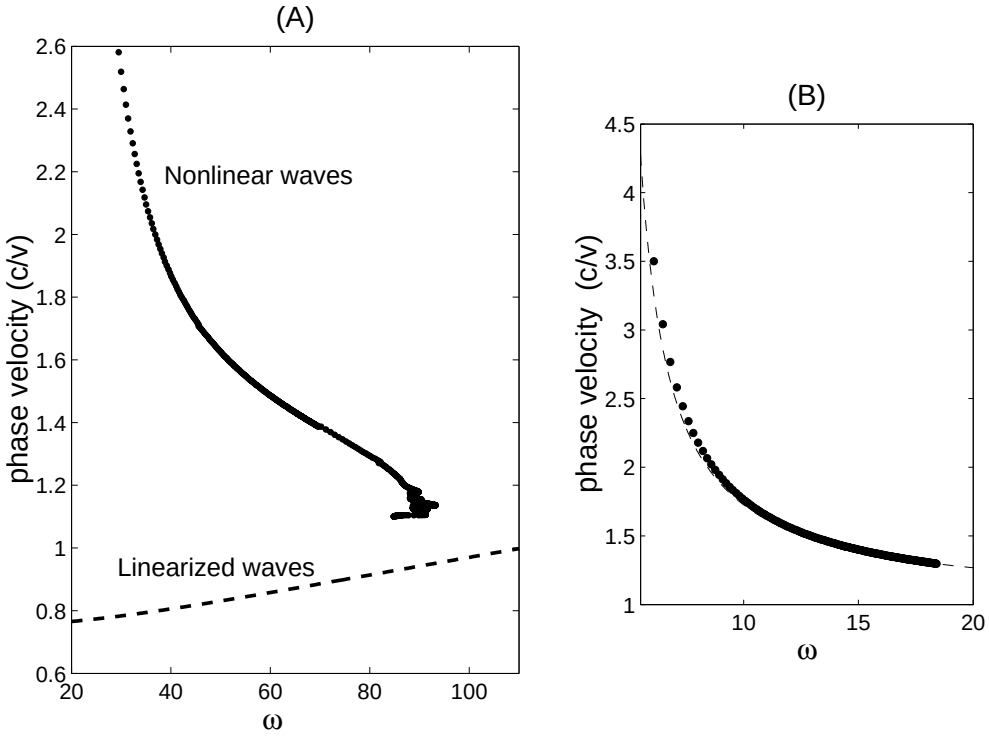

FIG. 6. (a) Phase velocity vs frequency ω for the case $e=50$, $v=1$, $D=0.003$ based on the numerical data of Fig. 5. There is evidently a maximum frequency. Perturbations near this frequency generate waves with a speed close to the flow velocity. The phase velocity for linearized small amplitude waves along the most unstable eigendirection is shown for comparison. Note that the cutoff frequency for small amplitude waves occurs precisely when their phase velocity reaches 1, as can be deduced from the dispersion relation. The maximum frequency for large amplitude waves (approximately 90) appears to be lower than the linear cutoff frequency of 110. In the gap between these two frequencies, the linearized analysis predicts a growing mode but Eq. (13) gives no solution with the correct frequency. (b) A similar plot for $e=2$, $v=1$, $D=0.0025$. In this case the phase velocity for nonlinear waves is very close to the linearized prediction, and becomes closer as the cutoff frequency of 18.36 is approached.

responding to these frequencies. In other words, there appears to be a nonlinear cutoff frequency which is lower than the linear one. Numerical results described below suggest that perturbations between these two frequencies are subject to a secondary instability.

C. Evolution and asymptotic wave forms of growing modes

In this section we display a few numerical solutions of the PDE (2) in which a small sinusoidal perturbation about the unstable fixed point grows with the downstream flow into a fully nonlinear wave solution governed by Eq. (13). A given solution of ODE (13) corresponds to a family of solutions of the PDE (2) which include traveling and stationary waves having the same value of Γ. In a sense, one can map any traveling onto a stationary wave with different values of the flow parameters but the same value of Γ and hence the same amplitude and shape. We have verified this numerically in the case of the weakly nonlinear FN model with $e=2$. If, however, the system is far from a Hopf bifurcation (for example, the FN system with $e=50$), some solutions at high values of Γ do not correspond to an easily observable stationary wave. This is because in the case of stationary waves ($c=0$) high values of Γ correspond to high values of ε, which are beyond the absolute instability threshold. In this case, initial conditions and temporal transients have a large influence on the final state in the bulk of the medium and the state is not so easily controlled by the upstream boundary condition. Therefore the highly nonkinematic wave forms seen in Fig. 4 do not correspond to standing waves that could be easily generated, but they can be generated as traveling waves. One then obtains high values of Γ by tuning the driving frequency to bring c close to v.

In Figs. 7–9 we display some examples of these waves in the FN system with $e=50$, $v=1$, and $D=0.003$, where the unstable fixed point is a node with two positive real eigenvalues. The predicted ω-c relation for these parameter values is shown in Fig. 6(a). The boundary condition is a sinusoidal disturbance $(X(0,t),Y(0,t))=(0.05\cos\omega t, 0.05\sin\omega t)$. The boundary forcing has components of equal size along both eigenvectors, but the component along the more unstable eigenvector of course grows faster. Figures 7 and 8 show waves generated by perturbations with $\omega=50$ and 80, respectively. These disturbances grow with downstream distance to resemble the wave forms of Fig. 4. Figure 9 shows the results of a perturbation with $\omega=85$, which is near the nonlinear cutoff frequency observed in Fig. 6. In this case, the perturbation initially grows along the more unstable eigendirection, but it penetrates only a small distance into the medium before breaking up. In the domain where the high-frequency wave exists, the disturbance appears to occur *only*

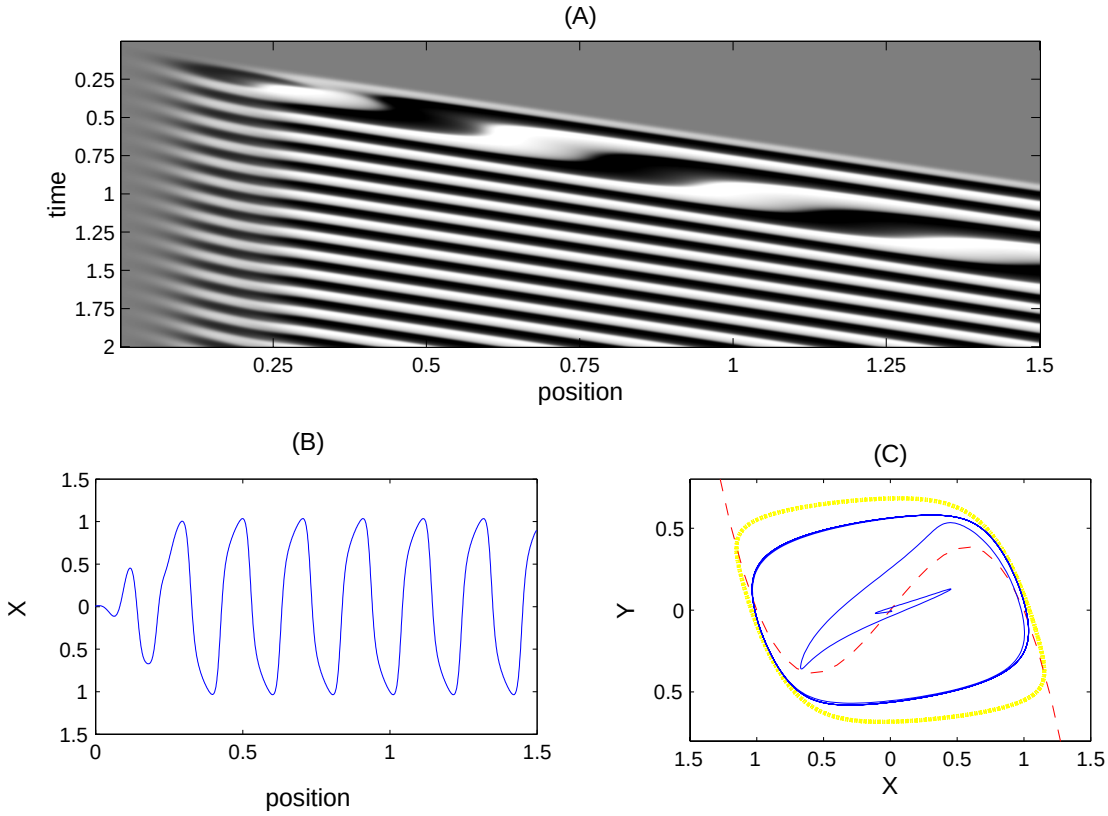

FIG. 7. (Color online) Waves generated by a sinusoidal perturbation with $\omega=50$ in the FN system with $e=50$, $v=1$, and $D=0.003$. The initial transient response to the switching on of the perturbation at $t=0$ is followed by a steady traveling wave with phase velocity $c \approx 1.6$, a value consistent with the ω-c relation plotted in Fig. 6. The corresponding value of Γ is 0.008. (a) is a space-time plot with a gray level proportional to $X(x,t)$. (b) shows $X(x,T)$ for a particular time T, while (c) shows the shape of the wave form in phase space by plotting $Y(x)$ against $X(x)$ at the same time. The orbit described by the underlying kinetics of the well-mixed system is shown as a lighter-colored line and the cubic nullcline (dashed line) is included for reference. Compare (b) and (c) to Fig. 4(a).

along the most unstable eigendirection. It never develops the loop in phase space that characterizes self-sustained oscillations. Instead it seems to behave as an imposed spatial pattern passively advected by the flow and simply stretched in phase space by the chemical dynamics until it breaks up and is replaced by a pattern of self-sustaining oscillations at a different frequency and wave number. Similar results were found for perturbations between $\omega \approx 85$ and the linear cutoff frequency of $\omega \approx 110$ (for $\omega > 110$ the perturbations are immediately damped). Evidently the waves within this frequency range are subject to a secondary instability. The patterns which arise after the high-frequency waves break up appear similar to the pulsating waves observed in Refs. [4] and [5]. The behavior of perturbations near the cutoff frequency in the case of an unstable node warrants further study.

V. CONCLUSIONS AND DISCUSSION

We have attempted to give a general framework for understanding the behavior of flow-distributed waves in one-dimensional open flows of oscillatory media without differential transport, aiming at generic results. First, we used linear stability analysis to examine the response to constant or sinusoidal forcing at the boundary, generalizing the results of [2,8,9]. We pointed out some particular features that occur when the unstable fixed point is a node rather than a focus. We then showed that the nonlinear behavior of periodic traveling or stationary waves reduces to a one-dimensional ODE (13) governed by the single parameter $\Gamma = D/(v-c)^2$, which has a physical interpretation as the strength of diffusive mixing between peaks and troughs of a particular wave. The ODE can be solved numerically to derive the wave forms and obtain a relation between the frequency of driving at the boundary and the wave number and/or phase velocity of the waves generated by the perturbation. We examined deviations of wave forms from the kinematic limit, noting qualitative differences between the quasiharmonic and relaxation cases.

We illustrated our formalism by applying it to the FitzHugh-Nagumo toy model, but the tools we developed here can be applied to other kinetic models, including those with multiple fixed points, period doubling, subcritical Hopf bifurcations, canards, and bistable behavior for which the linearized analysis is insufficient.

Some other questions have been left open. The behavior of traveling waves near the cutoff frequencies in the case of an unstable node may be a fruitful subject for further study. More generally, we have only hinted at the possibility of secondary instabilities that may affect FDO waves. Also, in

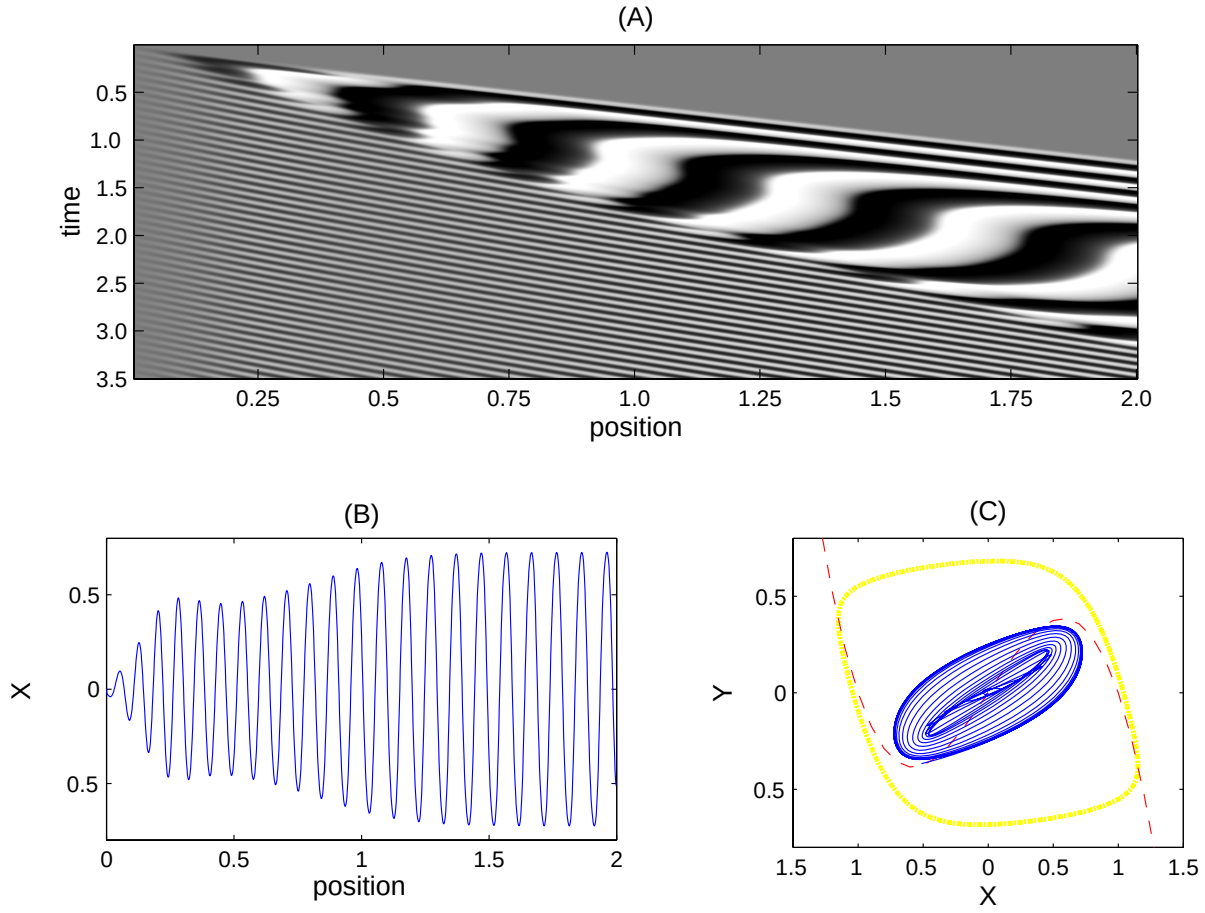

FIG. 8. (Color online) Waves generated by a perturbation with $\omega=80$ show a larger deviation from the kinematic limit. The waves have $c=1.27$ and $\Gamma=0.04$. Compare (b) and (c) with Fig. 4(b).

this work we have considered only regular traveling waves, not the pulsating waves observed in Refs. [4] and [5], although some of our numerical results (see Fig. 9) appeared to show pulsating waves arising from a secondary instability.

ACKNOWLEDGMENT

This work was supported by the NSERC of Canada.

APPENDIX A: THE FITZHUGH-NAGUMO MODEL: QUASISINUSOIDAL AND RELAXATION OSCILLATIONS

The FitzHugh-Nagumo (FN) model or van der Pol oscillator is defined[2] by [18,26,27]

$$\frac{dX}{dt}=e(X-X^3-Y),$$

$$\frac{dY}{dt}=-Y+aX+b. \tag{A1}$$

It is not a realistic model of any chemical system, since its state variables include negative values, but it serves as a useful toy model with many generic features seen in real chemical systems, including bistability, excitability, and oscillations of quasisinusoidal as well as relaxational character.

The nullclines are a cubic and a straight line. e is the ratio of time scales of motion along X and Y, a is the slope of the Y nullcline, and b is its intercept with the Y axis. Relaxation oscillations occur when e is large. The number and location of the fixed points depends on the Y nullcline, i.e., on values of a and b. There may be either one fixed point or three. In this paper we follow Ref. [13] in setting $b=0$, and additionally choose $a=10$, thus ensuring a single fixed point and excluding bistability, excitability, or canard transitions [31]. Only e is varied as a control parameter.

The Jacobian eigenvalues at the origin are given by

$$\lambda_{\pm}=\frac{e-1}{2}\pm\frac{1}{2}\sqrt{(1+e)^2-40e}. \tag{A2}$$

They are real and positive for all $e>e_{\mathrm{crit}}\approx 38$ and complex otherwise. Figure 10 shows the real and imaginary parts of the two eigenvalues $\lambda_{\pm}$ together with the angular frequency $\omega_{LC}=2\pi/T$ of the stable limit cycle which exists for all $e>1$. The Hopf bifurcation occurs at $e=1$ where $\mathrm{Re}(\lambda_{\pm})$ becomes positive. In the immediate vicinity of the Hopf bifurcation, the frequency of the limit cycle is identical to the

[2]This version of the model was used in Ref. [13].

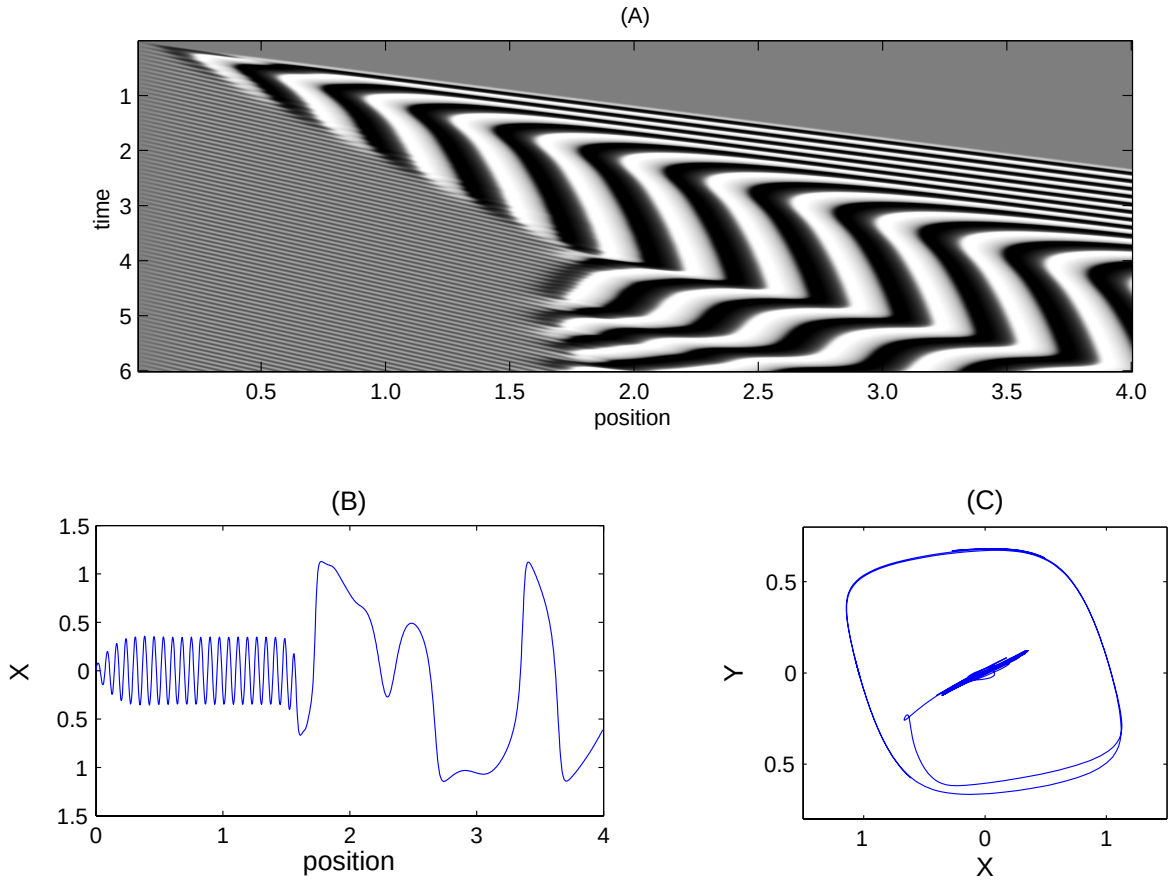

FIG. 9. (Color online) Boundary perturbation frequency $\omega = 85$. A high-frequency traveling wave, oscillating almost entirely along the most unstable eigendirection, penetrates a limited distance into the medium before giving way to a pattern of much longer, irregularly moving waves.

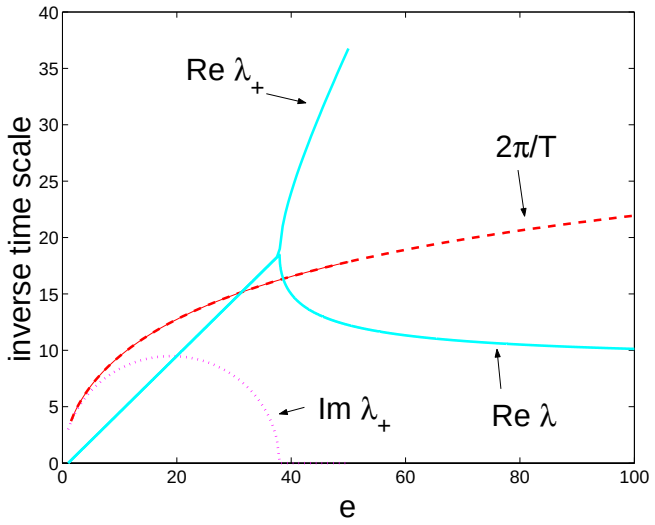

FIG. 10. (Color online) Inverse time scales as functions of e for $a = 10$. Dotted line, $\mathrm{Im}(\lambda_+)$; solid lines, $\mathrm{Re}(\lambda_\pm)$; dashed line, $2\pi/T$ for the limit cycle. At the critical value $e_c \approx 38$, the eigenvalues become real.

imaginary part $\mathrm{Im}(\lambda_+)$. At e_{crit}, however, $\mathrm{Im}(\lambda_+)$ vanishes and the eigenvalues become real. They are degenerate at the critical point but quickly become different as e increases further. Roughly speaking, the two real eigenvalues above e_{crit} correspond to two different inverse time scales: a slower one for motion in the Y direction and a faster one for motion in the X direction. It is this separation of time scales that distinguishes relaxation oscillations from quasisinusoidal ones. The frequency of relaxation oscillations is determined primarily by the *slower* of the two time scales. As e increases, the qualitative character of the oscillations changes from approximately sinusoidal to relaxation oscillations. Although there is a sudden change in the eigenvalues and eigenvectors near the fixed point at e_{crit}, the associated change in the nonlinear limit cycle is gradual.

APPENDIX B: NUMERICAL SOLUTIONS OF THE REDUCED ONE-DIMENSIONAL EQUATION

Here we discuss the solution of the reduced ODE (13)

$$0 = \mathbf{f}(\mathbf{u}) - \frac{d\mathbf{u}}{d\zeta'} + \Gamma_c \frac{d^2\mathbf{u}}{d\zeta'^2}.$$

In the kinematic limit $\Gamma \to 0$, this equation reduces to a first-order equation, identical in form to that of the dynamics of

the well-stirred system. Solutions of this first-order equation with general initial conditions approach the stable limit cycle of the well-stirred system. However, for any nonzero value of Γ the equation is second order and antidissipative,[3] so that the initial-value problem leads to unbounded solutions for most choices of initial conditions $\mathbf{u}(0)$ and $\mathbf{u}'(0)$. To exclude these unphysical solutions, a boundary condition must be imposed. Thus, the equation should be solved as a boundary-value problem on a finite interval $0<\zeta<L$. Our procedure was to impose a fixed boundary condition on the left, $\mathbf{u}(0)=\mathbf{u}_{\mathrm{in}}$, and a free boundary condition on the right, $\mathbf{u}'(0)=0$. In the case $c=0$ the boundaries correspond directly to the the physical boundaries of the plug-flow reactor.

For the examples studied, we found that for moderate values of Γ and for sufficiently large L the solutions of the boundary problem behave qualitatively like solutions of a first-order initial value problem with an attractor. In other words, after some transient behavior at small ζ which depends strongly on $\mathbf{u}_{\mathrm{in}}$, the solutions settle either to a fixed value or to a periodic behavior with an intrinsic period Λ,[4] which depends on Γ but does *not* depend sensitively on $\mathbf{u}_{\mathrm{in}}$ or on L. The free boundary condition on the right affects the solution only in a small interval near the right boundary, i.e., the boundary can be moved to a larger value of ζ without changing the solution on most of the interval $0<\zeta<L$. In the $c=0$ case, the entire solution, including the boundary transients, is physically meaningful as part of a stationary wave pattern in the reactor. For $c\neq 0$, boundary conditions at fixed ζ values are not directly equivalent to boundary conditions at fixed x, but the attractors reached by the solutions can be interpreted as the asymptotic shapes of traveling waves in the medium.

In order to obtain numerical solutions of the boundary value problem, we used a collocation algorithm included in the MATLAB software package [32]. This algorithm requires an initial guess for the solution which is then adjusted to satisfy the differential equations and the boundary conditions within a specified tolerance. For long solution intervals (large multiples of Λ) the algorithm may fail to converge unless the initial guess is close to the actual solution. We used two procedures for iteratively obtaining a solution.

(1) Use a solution of the initial value problem of the first-order, $\Gamma=0$ system as an initial guess for a relatively small value of Γ. Then increase Γ iteratively to the desired value, using each solution as the guess for the next value of Γ. This procedure was used, for example, to generate the solutions at a range of values of Γ in Fig. 5.

(2) Sometimes it is more convenient to approximate the solution with piecewise solutions on a series of overlapping intervals. The procedure is as follows: First, solve the boundary value problem with the desired boundary condition $\mathbf{u}_{\mathrm{in}}$ at $\zeta=0$ and free boundary conditions at a relatively small L which is neither too much larger nor too much shorter than Λ. Obtain a solution $\mathbf{u}_1(\zeta)$ on that interval. Then evaluate that solution at $\zeta=L/2$ and use $\mathbf{u}_1(L/2)$ as the boundary condition for a new solution on the interval $L/2<\zeta<3L/2$. Continue this procedure on a series of overlapping intervals. If L is not too large, then the initial trial solutions need not be close to the final ones, and if L is not too small they are not sensitive to the free boundary condition at the right, so that the overlapping solutions should be approximately the same except very near the boundaries. Stitched together, the piecewise solutions approximate a solution on a longer interval.

Large values of Γ (where large means significantly larger than $1/4\alpha$, the threshold of absolute instability in the $c=0$ case) often present computational challenges because the solutions become more sensitive to the right boundary condition, and large intervals were needed in order for an attractor to appear. This is the source of some of the numerical jitter in the data in Fig. 5.

[3] If the equation is rearranged to isolate the second-order term on one side, the analogy with the equation of motion of a point particle shows that the ''force'' contains an antidamping term, and the term $-\mathbf{f}(\mathbf{u})$ is also of the ''wrong'' sign, tending to push the particle away from the stable limit cycle of the well-mixed system.

[4] A chaotic attractor is also possible. We plan to discuss this in a future publication.

[1] S. P. Kuznetsov, E. Mosekilde, G. Dewel, and P. Borckmanns, J. Chem. Phys. **106**, 7609 (1997).
[2] P. Andresén, M. Bache, E. Mosekilde, G. Dewel, and P. Borckmanns, Phys. Rev. E **60**, 297 (1999).
[3] M. Kaern and M. Menzinger, Phys. Rev. E **60**, 3471 (1999).
[4] M. Kaern and M. Menzinger, Phys. Rev. E **61**, 3334 (2000).
[5] M. Kaern and M. Menzinger, J. Phys. Chem. A **106**, 4897 (2002).
[6] P. Andresén, E. Mosekilde, G. Dewel, and P. Borckmans, Phys. Rev. E **62**, 2992 (2000).
[7] M. Kaern and M. Menzinger, Phys. Rev. E **62**, 2994 (2000).
[8] J. R. Bamforth, S. Kalliadasis, J. H. Merkin, and S. K. Scott, Phys. Chem. Chem. Phys. **2**, 4013 (2000).
[9] J. R. Bamforth, J. H. Merkin, S. K. Scott, R. Tóth, and V. Gáspár, Phys. Chem. Chem. Phys. **3**, 1435 (2001).
[10] J. R. Bamforth, R. Tóth, V. Gáspár, and S. K. Scott, Phys. Chem. Chem. Phys. **4**, 1299 (2002).
[11] M. Kaern, M. Menzinger, and A. Hunding, Biophys. Chem. **87**, 121 (2000).
[12] M. Kaern, M. Menzinger, and A. Hunding, J. Theor. Biol. **207**, 473 (2000).
[13] M. Kaern, M. Menzinger, R. Satnoianu, and A. Hunding, Faraday Discuss. **192**, 295 (2001).
[14] M. Kaern, R. Satnoianu, A. P. Muñuzuri, and M. Menzinger, Phys. Chem. Chem. Phys. **4**, 1315 (2002).
[15] R. A. Satnoianu and M. Menzinger, Phys. Rev. E **62**, 113 (2000).
[16] R. A. Satnoianu, P. K. Maini, and M. Menzinger, Physica D **160**, 79 (2001).
[17] A. M. Turing, Philos. Trans. R. Soc. London, Ser. B **237**, 37 (1952).
[18] C. B. Muratov and V. V. Osipov, Phys. Rev. E **54**, 4860 (1996).

[19] A. B. Rovinsky and M. Menzinger, Phys. Rev. Lett. **69**, 1193 (1992); **70**, 778 (1993).
[20] R. Tóth, A. Papp, V. Gáspár, J. H. Merkin, S. K. Scott, and A. F. Taylor, Phys. Chem. Chem. Phys. **3**, 1435 (2001).
[21] S. M. Tobias, M. R. E. Proctor, and E. Knobloch, Physica D **113**, 43 (1998).
[22] W. van Saarlos (unpublished).
[23] M. R. E. Proctor, S. M. Tobias, and E. Knobloch, Physica D **145**, 191 (2000).
[24] A. Couairon and J.-M. Chomaz, Physica D **158**, 129 (2001).
[25] A. Tsameret and V. Steinberg, Phys. Rev. E **49**, 1291 (1994); K. L. Babcock, D. S. Cannell, and G. Ahlers, Physica D **61**, 40 (1992).
[26] S. P. Dawson, M. V. D'Angelo, and J. E. Pearson, Phys. Lett. A **265**, 346 (2000).
[27] A. Hagberg and E. Meron, Chaos **4**, 477 (1994).
[28] R. J. Deissler, J. Stat. Phys. **40**, 371 (1985); **54**, 1459 (1989).
[29] G. B. Whitham, *Linear and Nonlinear Waves* (Wiley, New York, 1973).
[30] P. Huerre, in *Instabilities and Nonequilibrium Structures*, edited by E. Tirapegui and D. Villaroel (Reidel, Dordrecht, 1987), pp. 141–177.
[31] E. Benoit, J. L. Callot, F. Diener, and M. Diener, Collect. Math. **32**, 37 (1981); M. Diener and T. Poston, in *Chaos and Order in Nature*, edited by E. Haken (Springer-Verlag, Berlin, 1981), pp. 279–289; M. Diener, Math. Intell. **6**, 38 (1984); B. Peng, V. Gaspar, and K. Showalter, Philos. Trans. R. Soc. London, Ser. A **337**, 275 (1991).
[32] L. F. Shampine, M. W. Reichelt, and J. Kierzenka, ftp://ftp.mathworks.com/pub/doc/papers/bvp/